XIII International Conference on Computational Plasticity. Fundamentals and Applications
COMPLAS XIII
E. Oñate, D.R.J. Owen, D. Peric and M. Chiumenti (Eds)

MRCT ELEMENT WITH A DISLOCATION BASED PLASTICITY MODEL

HAO QIN*, LARS-ERIK LINDGREN*

* Luleå University of Technology
971 76 Luleå, Sweden
e-mail: hao.qin@ltu.se, lel@ltu.se, web page: http://www.ltu.se

Key words: Physically based model, Dislocation density, Higher order continuum theory.
Abstract. The multiresolution continuum theory (MRCT) [1] has been established to link the material's macroscopic behaviour with its microstructural inhomogeneities. Additional kinematic variables in addition to the conventional macroscopic displacement field are added to account for microstructural deformations at multiple microscales. Metal plasticity is associated with interaction of motion of dislocations and microstructures. A Dislocation density based material model [2] calibrated and validated for AISI 316L at different temperatures and strain rates is used as the macroscopic constitutive equation of the MRCT element. We investigated particularly how the changing property of the microdomain with changing temperature affects the macroscopic behaviours of the material.

1 INTRODUCTION

In classical continuum description, the material's response at a point **x** is solely determined by the deformation at this point. It can integrate and catch some aspects of the underlying material microstructure, but the size dependent material response cannot be accounted for, the scale effect is lost during the homogenization procedure.

The multiresolution continuum theory (MRCT) [3-5] is a higher order continuum theory that enhances the macroscopic description of a material with influence from a neighborhood on the deformation. This neighborhood, microdomain, is associated with a length scale and also with constitutive models connecting higher order gradients and stresses as indicated below. They enrich the traditional homogenization procedure and remedy the mesh dependency when simulating localization problems.

The inelastic deformation depends on the interaction between dislocations and the microstructure of the material. This structure is evolving during the deformation and is affected by the strain rate and temperature. The dislocation density model [2] is a physically based model that takes the varying strain, strain rate, temperature and as well the changing microstructures, dislocation density etc, into account. The dislocation density model used in the current paper is calibrated and validated for AISI 316L at different temperatures and strain rates and used as the macroscopic constitutive equation of the MRCT element.

The paper also includes and evaluation of the effect of changing properties of the microdomain on the macroscopic behaviours of the material.

2 MULTIRESOLUTION CONTINUUM THEORY (MRCT)

A material point **x** in the higher order continuum theory is considered itself as an infinitesimal continuum, which has an inner structure that can be modeled as a sequence of

nested microdomains. Each centered at this point **x** and each represents a particular length scale l^i. The velocity field in the microdomain is assumed to be linear as

$$ {}_m\mathbf{l}^i = \mathbf{l}^i(\mathbf{x}) + \mathbf{g}^i(\mathbf{x}) \cdot \mathbf{y}^i \tag{1} $$

where ${}_m\mathbf{l}^i$ is the local velocity gradient in each microdomain *i*. $\mathbf{y}^i$ is the local coordinate in the *i*th microdomain relative to the domain center. The term $\mathbf{l}^i$ is the volume average of the local velocity gradient and $\mathbf{g}^i$ is the gradient of micro-velocity gradient.

The Hill-Mandel principle is used to extend to traditional virtual internal power to account for both homogeneous deformation at the macroscopic scale and inhomogeneous deformation arising from multiple length scales. During the deformation the rotations of the microdomains with respect to the macroscopic domain are ignored. The total virtual internal power integrated over the entire body is written as:

$$ \delta p_{\text{int}} = \delta p_{\text{int}}^{\text{hom}} + \delta p_{\text{int}}^{\text{inh}} = \int_\Omega \left(\boldsymbol{\sigma}^0 : \delta \mathbf{d}^0 + \sum_{i=1}^{N} \left(\boldsymbol{\beta}^i : \delta\left(\mathbf{d}^i - \mathbf{d}^0 \right) + \mathbf{m}^i : \delta \mathbf{g}_d^i \right) \right) d\Omega \tag{2} $$

where $\mathbf{d}^0$ is the spatial rate of deformation and $\boldsymbol{\sigma}^0$ is the Cauchy stress tensor at the macroscale. Two new stress measures have been introduced above: (1) the microstress $\boldsymbol{\beta}^i$ as the power conjugate to the microscopic rate of deformation ($\mathbf{d}^i - \mathbf{d}^0$) and (2) the microstress couple $\mathbf{m}^i$ as the power conjugate to $\mathbf{g}_d^i$ which is the symmetric part of the quantity $\mathbf{g}^i$. Thus we have $\mathbf{d}^0, (\mathbf{d}^i - \mathbf{d}^0), \mathbf{g}_d^i$ as the knematic variables and $\boldsymbol{\sigma}^0, \beta^i, \mathbf{m}^i$ as the generalized stresses. *N* is total number of scales.

For simplicity, we leave out the external virtual power as well as inertial effects. Integrating Eq. (2) by parts and applying the divergence therom, we have

$$ \begin{aligned} \delta p_{\text{int}} = &-\int_\Omega \left\{ \nabla \left(\sigma^0 - \sum_{i=1}^{N} \beta^i \right) \cdot \delta \mathbf{v}^0 + \sum_{i=1}^{N} \left(\nabla \mathbf{m}^i - \beta^i \right) : \delta \mathbf{d}^i \right\} d\Omega \\ &+ \int_S \left(\sigma^0 - \sum_{i=1}^{N} \beta^i \right) \cdot \mathbf{n} \cdot \delta \mathbf{v}^0 dS + \int_S \sum_{i=1}^{N} \left(\mathbf{m}^i \cdot \mathbf{n} \right) : \delta \mathbf{d}^i dS = 0. \end{aligned} \tag{3} $$

$\boldsymbol{\delta}\mathbf{v}^0$ is the macroscale virtual velocity, which arises from integrating by parts the power conjugate pairs at each scale. **n** and *S* arise from the application of Gauss's theorem, *S* is the surface enclosing the volume and **n** is the outward pointing unit normal.

By the application of the principle of virtual power, Eq. (3) should be valid for all admissible velocity fields. Thus, we obtain the multiresolution continuum equilibrium equations as

$$ \begin{aligned} \nabla \cdot \left(\boldsymbol{\sigma}^0 - \sum_{i=1}^{N} \boldsymbol{\beta}^i \right) = 0 \\ \nabla \cdot \mathbf{m}^i - \boldsymbol{\beta}^i = 0 \end{aligned} \tag{4} $$

with boundary conditions:

$$\left(\boldsymbol{\sigma}^0 - \sum_{i=1}^{N} \boldsymbol{\beta}^i\right) \cdot \mathbf{n} = 0 \qquad (5)$$
$$\mathbf{m}^i \cdot \mathbf{n} = 0$$

3 IMPLICIT MRCT 3D ELEMENT.

3.1 MRCT element formulations.

A 3D implicit MRCT element [6] has been implemented in a general finite element program FEAP [7]. Only one subscale is considered in the current implementation.

The generalized strain rate vector for the kinematic variables in Eq.(2) is calculated as

$$\Delta = \begin{bmatrix} \mathbf{d}^0 \\ \mathbf{d}^1 - \mathbf{d}^0 \\ \mathbf{g}_d^1 \end{bmatrix} = \begin{bmatrix} \mathbf{B}^0 & 0 \\ -\mathbf{B}^0 & \mathbf{N}^1 \\ 0 & \mathbf{G}^1 \end{bmatrix} \begin{bmatrix} \mathbf{v}^0 \\ \mathbf{d}^1 \end{bmatrix} = \mathbf{Q}\mathbf{v} \qquad (6)$$

where $\mathbf{B}^0$ is the strain-displacement matrix at the macroscopic scale. $\mathbf{N}^1 = \mathbf{N}^0$ is the shape function matrix. $\mathbf{G}^1$ is the strain-displacement matrix for the gradient terms.

The generalized stress vector is written as

$$\boldsymbol{\Sigma} = \begin{bmatrix} \boldsymbol{\sigma}^0 \\ \boldsymbol{\beta}^1 \\ \mathbf{m}^1 \end{bmatrix} \qquad (7)$$

The MRCT internal force vector and the consistent tangent matrix is given below

$$\mathbf{f}_{\text{int}} = \int_\Omega \mathbf{Q}^T \Sigma \, d\Omega = \int_\Omega \begin{bmatrix} \left(\mathbf{B}^0\right)^T \left(\boldsymbol{\sigma}^0 - \boldsymbol{\beta}^1\right) \\ \left(\mathbf{N}^1\right)^T \boldsymbol{\beta}^1 + \left(\mathbf{G}^1\right)^T \mathbf{m}^1 \end{bmatrix} d\Omega. \qquad (8)$$

$$\mathbf{K} = \int_\Omega \begin{bmatrix} \mathbf{K}^0 + \left(\mathbf{B}^0\right)^T \mathbf{C}_\beta^{al1} \mathbf{B}^0 & -\left(\mathbf{B}^0\right)^T \mathbf{C}_\beta^{al1} \mathbf{N}^1 \\ -\left(\mathbf{N}^1\right)^T \mathbf{C}_\beta^{al1} \mathbf{B}^0 & \left(\mathbf{N}^1\right)^T \mathbf{C}_\beta^{al1} \mathbf{N}^1 + \left(\mathbf{G}^1\right)^T \mathbf{C}_{\text{m}}^{al1} \mathbf{G}^1 \end{bmatrix} d\Omega.$$

where

$$\mathbf{K}^0 = \mathbf{B}^{0T} \left(\mathbf{C}_\sigma^{al} - \tilde{\boldsymbol{\sigma}}\right) \mathbf{B}^0 + \mathbf{G}^{0T} \hat{\boldsymbol{\sigma}} \mathbf{G}^0 \qquad (9)$$

and $\mathbf{C}_\sigma^{al}, \mathbf{C}_\beta^{al1}, \mathbf{C}_{\text{m}}^{al1}$ are algorithmic moduli at different scales. The detailed expressions of $\tilde{\boldsymbol{\sigma}}$, $\hat{\boldsymbol{\sigma}}$ and $\mathbf{G}^0$ are listed in [8] .

3.2 MRCT constitutive relations

A hypoelastic-plastic approach is used in the stress updating algorithm and the formulation accommodates large strains. The multiresolution continuum elastic matrix $\mathbf{C}$ relates the objective rates of the generalized stress vector and the elastic part of the generalized strain rate vector

$$\Sigma^{\nabla} = \mathbf{C} \cdot \Delta^{e} \tag{10}$$

$\mathbf{C}$ is written as

$$\mathbf{C} = \begin{bmatrix} \mathbf{C}_{\sigma} & 0 & 0 \\ 0 & \mathbf{C}^{1}_{\beta} & 0 \\ 0 & 0 & \mathbf{C}^{1}_{\mathrm{m}} \end{bmatrix} \tag{11}$$

$\mathbf{C}_{\sigma}$ is the conventional elasticity tensor (Hooke's law), $\mathbf{C}^{1}_{\beta}$ and $\mathbf{C}^{1}_{\mathrm{m}}$ are the elastic moduli in the microdomain given by

$$\mathbf{C}^{1}_{\beta} = \frac{1}{\Omega^{1}} \int_{\Omega^{1}} {}_{m}\mathbf{C}^{a}\, d\Omega = \mathbf{C}^{a} \tag{12}$$

$$\mathbf{C}^{1}_{\mathrm{m}} = \frac{1}{\Omega^{1}} \int_{\Omega^{1}} {}_{m}\mathbf{C}^{a} \otimes \mathbf{y} \otimes \mathbf{y}\, d\Omega = \mathbf{C}^{a} \otimes \frac{\left(l^{1}\right)^{2}}{12}\mathbf{I}$$

$\mathbf{I}$ is the identity matrix, $\mathbf{C}^{a}$ is the volume average of local elasticity tensor in the microdomain. The elastic moduli in the microdomain used in Eq.(12) is taken as $\mathbf{C}^{a} = \mathbf{C}_{\sigma} / 10$ based on [9]. The length scale parameter l^{1} has been directly incorporated into the multiresolution continuum constitutive relations.

A J_2 plasticity is used to model the finitely deformed materials at the macroscopic scale. A dislocation density based material model [2] is used to model the macroscopic flow stress. A detailed description about the model will be given in the next section. The subscale is assumed to be pure elastic in the current study.

4 DISLOCATION DENSITY MODEL

4.1 Flow stress.

The dislocation density based models are physically based models where the underlying physical processes during the deformation are used to construct the constitutive equations. An overview of the different deformation mechanisms are given in [10] .

The flow stress in current model consists of two parts

$$\sigma_{y} = \sigma_{G} + \sigma^{*} \tag{13}$$

where σ_{G} is an athermal stress contribution which is due to long-range interactions with the dislocation substructure. It is written as

$$\sigma_G = m\alpha Gb\sqrt{\rho_i} \tag{14}$$

where m is the Taylor orientation factor. α is a proportionality factor, G is temperature dependent shear modulus, b is Burger's vector.

σ^* is the short-range stress component

$$\sigma^* = \tau_0 G\left(1-\left(\frac{kT}{\Delta f_0 G b^3}\ln\left(\frac{\dot{\bar{\varepsilon}}_{ref}}{\dot{\bar{\varepsilon}}^p}\right)\right)^{1/q}\right)^{1/p} \tag{15}$$

where τ_0 is the athermal flow strength that must be exceeded in order to move the dislocation across the barrier without aid of thermal energy. k is the Boltzmann's constant. Δf_0 is the free energy required to overcome the lattice resistance or obstacles without aid from external stress. $\dot{\bar{\varepsilon}}_{ref}$ is the reference strain rate. q and p are parameters with the condition

$$\begin{aligned} 0 \le p \le 1 \\ 1 \le q \le 2 \end{aligned} \tag{16}$$

4.2 Evolution equations.

The dislocation processes include generation, annihilation, immobilization and remobilization of dislocations. The evolution equation is written in a general form as

$$\dot{\rho}_i = \dot{\rho}_i^{(+)} - \dot{\rho}_i^{(-)} \tag{17}$$

The mobile dislocation density is assumed to be independent of stress and strain and is much smaller than the immobile dislocation density. Subscript i represents the immobile dislocation density.

The hardening term is assumed to be proportional to the effective plastic strain rate

$$\dot{\rho}_i^{(+)} = \frac{m}{b}\frac{1}{\Lambda}\dot{\bar{\varepsilon}}^p \tag{18}$$

where the mean free path Λ is assumed to be the contribution from the grain size g and dislocation subcell size s in current model

$$\frac{1}{\Lambda} = \frac{1}{g} + \frac{1}{s}\cdots \tag{19}$$

and other contributions may also be included. The equation corresponds to assuming additive contributions to immobilization of dislocations. The grain size g is assumed to be constant and the evolution of the subcell size is written as

$$s = K_c\frac{1}{\sqrt{\rho_i}} \tag{20}$$

where K_c is a temperature dependent parameter.

There are different processes that contribute to the reduction of the dislocation density. We

include a dynamic recovery contribution that is proportional to the immobile dislocation density

$$\dot{\rho}_i^{(-)} = \Omega \rho_i \dot{\bar{\varepsilon}}^p \tag{21}$$

where Ω is a temperature dependent material parameter. A model for recovery by climb has also been included as

$$\dot{\rho}_i^{(-)} = 2c_\gamma D_v \frac{c_v}{c_v^{eq}} \frac{Gb^3}{kT} \left(\rho_i^2 - \rho_{eq}^2 \right) \tag{22}$$

where c_γ is a calibration parameter, D_v is diffusivity, c_v^{eq} is the thermal equilibrium vacancy concentration and c_v is the fraction of vacancies. The diffusivity is scaled due to generation of excess vacancies. This is done by multiplying D_v by the quotient of c_v divided by c_v^{eq}. ρ_{eq} is the equilibrium value towards which the dislocation density decreases. The diffusivity D_v is written as

$$D_v = D_{v0} e^{\left(-\frac{Q_{vf} + Q_{vm}}{kT} \right)} \tag{23}$$

where Q_{vf} is the activation energy for forming a vacancy and Q_{vm} is the vacancy migration and

$$D_{v0} = D_{vm0} e^{\left(\frac{\Delta S_{vf}}{k} \right)} \tag{24}$$

where D_{vm0} is a reference diffusivity and ΔS_{vf} is the increase in entropy when a vacancy is created.

The equilibrium vacancy concentration c_v^{eq} is written as

$$c_v^{eq} = e^{\left(\frac{\Delta S_{vf}}{k} \right)} e^{\left(-\frac{Q_{vf}}{kT} \right)} \tag{25}$$

The evolution of the vacancy concentration (generation and recovery) is modeled with the following equation for mono-vacancy evolution [11]

$$\dot{c}_v = \left(\chi \frac{\Omega_0}{Q_{vf}} \sigma_y + \varsigma \frac{c_j \Omega_0}{4b^3} \right) \dot{\bar{\varepsilon}}^p - D_{vm} \left(\frac{1}{s^2} + \frac{1}{g^2} \right) \left(c_v - c_v^{eq} \right) + \dot{c}_v^{eq} \tag{26}$$

χ is a material parameter, Ω_0 is the atomic volume and c_j is the concentration of thermal jogs. The latter is written as

$$c_j = e^{\left(-\frac{Q_{fj}}{kT} \right)} \tag{27}$$

where the formation energy Q_{fj} is

$$Q_{fj} = \frac{Gb^3}{4\pi(1-\nu)} \tag{28}$$

and ν is the Poissons's ratio.

Parameter ς is calculated as

$$\varsigma = \begin{cases} 0.5 - \varsigma_0 c_j & if\ c_j \le 0.5/\varsigma_0 \\ 0 & if\ c_j > 0.5/\varsigma_0 \end{cases} \quad (29)$$

where $\varsigma_0 = 10$.

D_{vm} is the vacancy migration for vacancy annihilation and is calculated as

$$D_{vm} = D_{vm0} e^{\left(-\frac{Q_{vm}}{kT}\right)} \quad (30)$$

The rate of change in vacancy concentration due change in temperature $\dot{c}_v^{eq}$ is written as

$$\dot{c}_v^{eq} = c_v^{eq}\left(\frac{Q_{vf}}{kT^2}\right)\dot{T} \quad (31)$$

The detailed the stress updating procedure is given in [2].

5 EXAMPLES

The model is calibrated with the compression test data of 316L stainless steel at 4 temperatures 20°C, 400°C, 800°C and 1300°C respectively and at the strain rate 0.01s^{-1}. The used model parameters are given in [2]. The calibration result is shown in Figure 1. The symbols are the experimental measurements and the solid lines are predicted by the model.

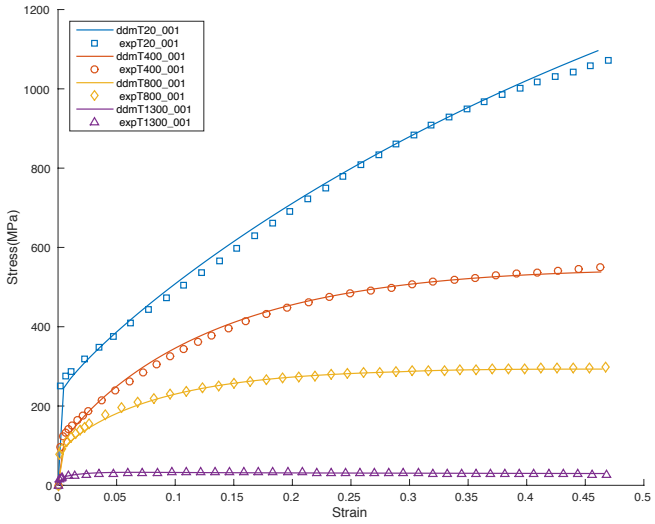

Figure 1: Dislocation density model calibrated with the experimental data.

A 3D plate is loaded in tension by prescribing the counter propagating motions at each ends, only 1/8 of the geometry is modeled due to symmetry. The length and the height of the plate in the x and y directions are 10 mm and 12 mm, respectively. The thickness of the plate is 1 mm. The mesh is show in Figure **2**.

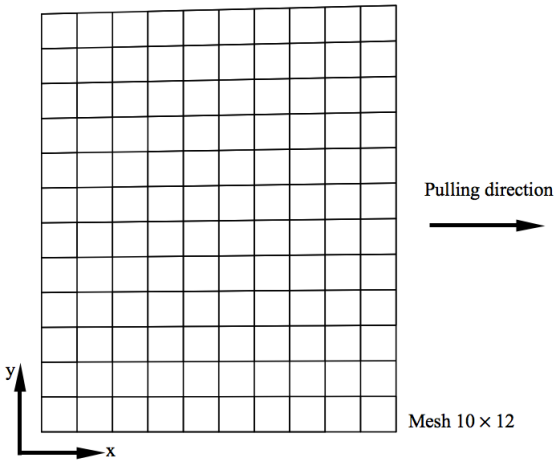

Figure 2: 3D plate.

The effect of the changing properties of the microdomain of the MRCT element on the macroscopic behavior has been studied. We prescribed the temperature to be 400°C for all cases below. The x-component of the stress along the bottom edge of the plate is shown in Figure **3**. The different curves correspond to different properties of the microdomain with a fixed length scale of 1. C1=C0/100, for example, means that $\mathbf{C}^a$ in Eq. (12) is of 1/100 of $\mathbf{C}_\sigma$.

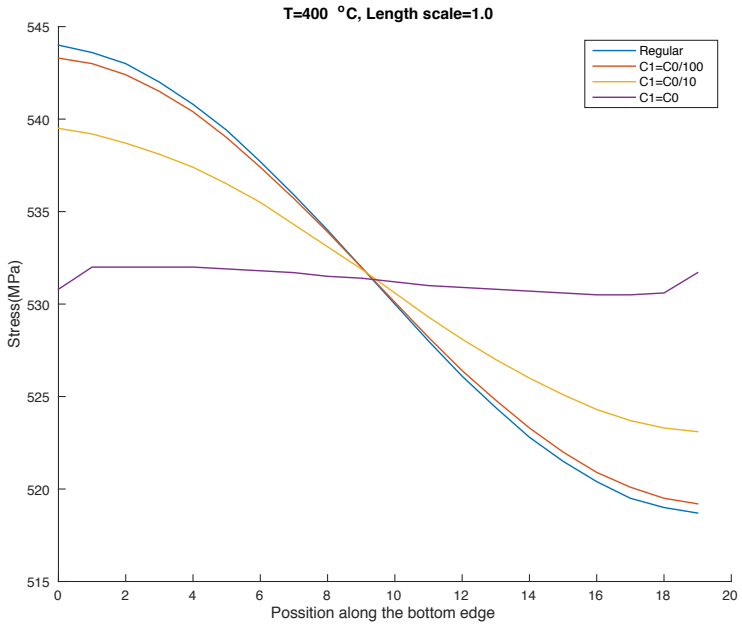

Figure 3 x-component of stress along the bottom edge of the plate predicted at the end of the elongation with different properties of the microdomain at 400°C with a fixed length scale.

The same stress has been plotted in Figure **4** for different length scales and with $\mathbf{C}^a$ fixed as 1/10 of $\mathbf{C}_\sigma$. LS=0.5, 1.0 and 5.0 simply means length scale is equal to 0.5, 1.0 and 5.0,

respectively. The element size for the mesh shown in Figure **2** is 1, so the length scale used in the simulation is smaller, equal or larger than the element size.

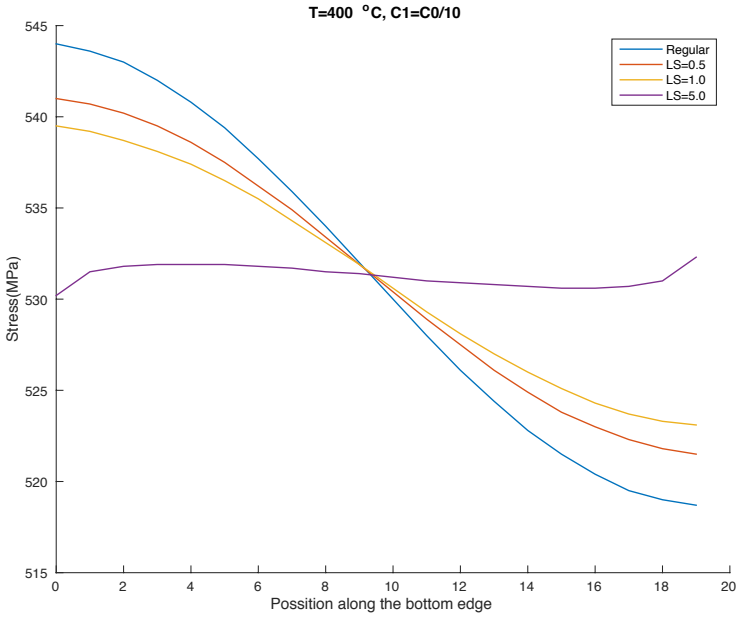

Figure 4 x-component of stress along the bottom edge of the plate predicted at the end of the elongation with different length sclaes at 400°C with a fixed C1.

The previous two figures show that there is a similar influence of the properties of the microdomain on the macroscopic behavior. Both increasing the microscopic stiffness or the length scale parameter stiffens the microdomain and prevents the localization as is shown in the figures.

The MRCT element can give mesh independent results [6] . A simple damage model was applied at the macroscopic scale of the MRCT element. The mesh is discretized as shown in Figure **5** with the name *m1012, m2024, m4048 and m8096* from left to right respectively, which indicates how much the mesh is refined.

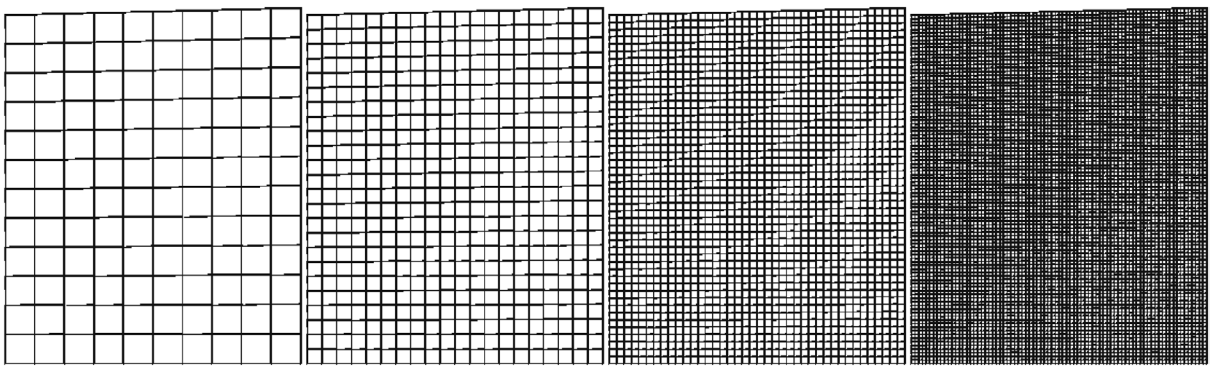

Figure 5 Refined mesh.

The mesh dependent force displacement curves predicted by the conventional continuum element, i.e. no microdomain, are shown in Figure **6**.

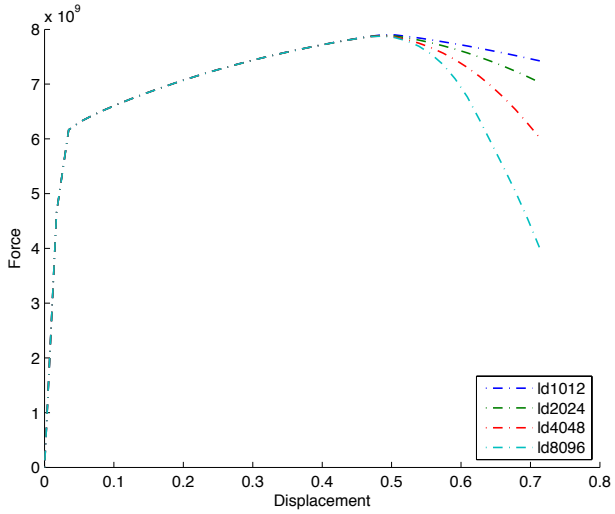

Figure 6 Mesh dependent results.

The mesh force displacement curves predicted by MRCT element with different length scales are shown in Figure **7** and Figure **8**. When using length scale of 1, the results given by the two finer meshes *m4048* and *m8096* are getting closer, but the discrepancy between the meshes can still be seen. When using length scale of 2, then we have the mesh independent results for all 4 meshes as opposed to the results predicted by the conventional continuum method as shown in Figure **6**.

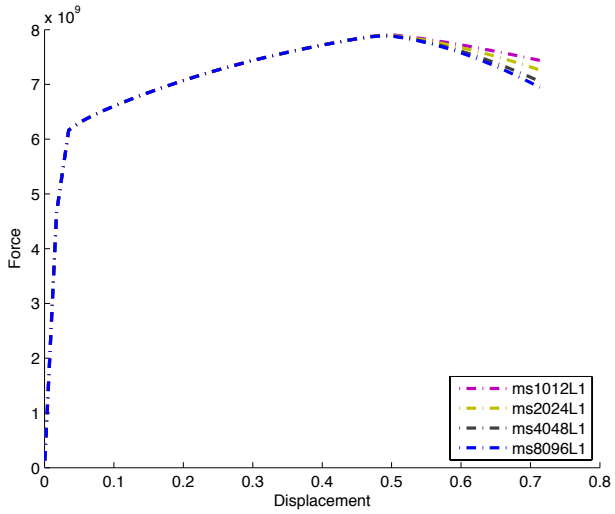

Figure 7 Force displacement plot predicted by MRCT with length scale of 1.

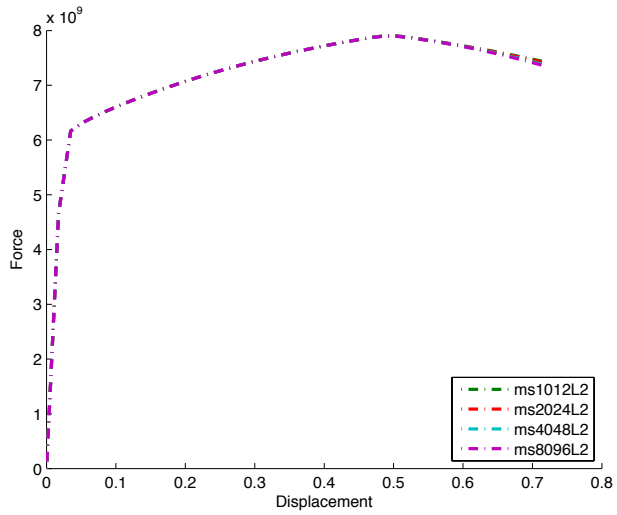

Figure 8 Force displacement plot predicted by MRCT with length scale of 1.

6 CONCLUSIONS AND DISCUSSIONS

An implicit MRCT element has been formulated and implemented in [6] . It can give mesh independent results for localization problem provided an appropriate length scale is chosen.

A dislocation density model has now been implemented in the macroscopic part of the MRCT element as it has been found to be better than the more common Johnson-Cook model in machining simulations [12, 13] . The combination of this model together with the capability of the element to handle localization problems makes the formulation a candidate for machining simulations.

The effects of the changing length scale and that of the changing microscopic properties on the macroscopic behaviors are studied and demonstrated at 400^{o}C with strain rate 0.01s^{-1}. The deformation in the microdomain is triggered by the non-uniform macroscopic deformations. It resists these gradients and thereby stabilizes the solutions in case of localization. Increasing the microscopic stiffness stiffens the microdomain and thus assists in reducing the gradients of the macroscopic deformation giving less localization. At least the elastic properties of the microdomain cannot be taken the same as for the macroscopic behavior as then it will resist localization too much as shown in Figure 3. Thus they are part of a calibration procedure.

7 REFERENCES

[1] F. Vernerey, W. K. Liu and B. Moran. Multi-scale micromorphic theory for hierarchical materials. *J. Mech. Phys. Solids 55(12),* pp. 2603-2651. 2007. . DOI: http://dx.doi.org/10.1016/j.jmps.2007.04.008.

[2] L. Lindgren, K. Domkin and S. Hansson, "Dislocations, vacancies and solute diffusion in physical based plasticity model for AISI 316L," *Mech. Mater.,* vol. 40, pp. 907-919, 2008.

[3] W. K. Liu and C. McVeigh. Predictive multiscale theory for design of heterogeneous materials. *Comput. Mech. 42(2),* pp. 147-170. 2008.

[4] C. McVeigh and W. K. Liu. Linking microstructure and properties through a predictive multiresolution continuum. *Comput. Methods Appl. Mech. Eng. 197(41–42),* pp. 3268-3290. 2008. . DOI: http://dx.doi.org/10.1016/j.cma.2007.12.020.
[5] C. McVeigh, F. Vernerey, W. K. Liu and L. Cate Brinson. Multiresolution analysis for material design. *Comput. Methods Appl. Mech. Eng. 195(37–40),* pp. 5053-5076. 2006. . DOI: 10.1016/j.cma.2005.07.027.
[6] H. Qin, L. Lindgren, W. K. Liu and J. Smith, "Implicit finite element formulation of multiresolution continuum theory," *Comput. Methods Appl. Mech. Eng.,* .
[7] O. C. Zienkiewicz and R. L. Taylor. *The Finite Element Method: Solid Mechanics* 20002.
[8] M. Crisfield and J. L. Tassoulas. Non-linear finite element analysis of solids and structures, volume 1. *J. Eng. Mech. 119(7),* pp. 1504-1505. 1993.
[9] F. Vernerey, W. K. Liu and B. Moran. Multi-scale micromorphic theory for hierarchical materials. *J. Mech. Phys. Solids 55(12),* pp. 2603-2651. 2007.
[10] H. Frost and M. Ashby, "Deformation-mechanism maps for pure iron, two austenitic stainless steels, and a low-alloy ferritic steel," in *Fundamental Aspects of Structural Alloy Design*Anonymous Springer, 1977, pp. 27-65.
[11] M. Militzer, W. Sun and J. Jonas, "Modelling the effect of deformation-induced vacancies on segregation and precipitation," *Acta Metallurgica Et Materialia,* vol. 42, pp. 133-141, 1994.
[12] A. Svoboda, D. Wedberg and L. Lindgren, "Simulation of metal cutting using a physically based plasticity model," *Modell Simul Mater Sci Eng,* vol. 18, pp. 075005, 2010.
[13] D. Wedberg, A. Svoboda and L. Lindgren, "Modelling high strain rate phenomena in metal cutting simulation," *Modell Simul Mater Sci Eng,* vol. 20, pp. 085006, 2012.